remote sensing

MDPI

Article

Monitoring and Integrating the Changes in Vegetated Areas with the Rate of Groundwater Use in Arid Regions †

Mona Morsy [1,2,3], Silas Michaelides [4,*], Thomas Scholten [3] and Peter Dietrich [1,5]

[1] Environmental and Engineering Geophysics Department, Monitoring and Exploration Technologies Helmholtz Center for Environmental Research—UFZ, Permoserstr. 15, 04318 Leipzig, Germany
[2] Geology Department, Faculty of Science, Suez Canal University, Ismailia 41522, Egypt
[3] Department of Geosciences, Soil Science and Geomorphology, University of Tübingen, Rümelinstr. 19-23, 72070 Tübingen, Germany
[4] Eratosthenes Centre of Excellence, Limassol 3036, Cyprus
[5] Center for Applied Geoscience, University of Tübingen, Schnarrenbergstr. 94-96, 72076 Tübingen, Germany
* Correspondence: silas.michaelides@eratosthenes.org.cy; Tel.: +357-994-93072
† This paper is an extended version of the abstract: Monitoring and integrating the expansion of vegetated areas with the rate of groundwater use in arid regions. European Geosciences Union, General Assembly, April 2022. https://doi.org/10.5194/egusphere-egu22-11902.

Abstract: Frequent water table measurements are crucial for sustainable groundwater management in arid regions. Such monitoring is more important in areas that are already facing an acute problem with excessive groundwater withdrawal. In the majority of these locations, continuous readings of groundwater levels are lacking. Therefore, an approximate estimate of the rate of increase or decrease in water consumption over time may serve as a proxy for the missing data. This could be achieved by tracking the changes in vegetated areas that generally correlate with changes in the rate of water use. The technique proposed in this paper is based on two remote sensing datasets: Landsat 7 and 8 from 2001 to 2021, and Sentinel 2A from 2015 to 2021, as well as five vegetation indices: Normalized Difference Vegetation Index (NDVI), Renormalized Difference Vegetation Index (RDVI), Soil Adjusted Vegetation Index (SAVI), Enhanced Vegetation Index (EVI), and Transformed Vegetation Index (TVI). The findings have shown that the datasets chosen performed best for small-scale land farms at the research location, which was chosen to be the El-Qaa plain, in the southwestern corner of the Sinai Peninsula in Egypt. Landsat 7 data with a resolution of 30 m revealed a substantial increase in land farms from 2.9 km^2 in 2001 to 23.3 km^2 in 2021. By using the five indices based on Sentinel 2A data, vegetated areas were categorized as heavy, moderate, or light. In addition, the expansion of each class area from 2015 to 2021 was tracked. Additionally, the NDVI index was modified to better reflect the arid environment (subsequently naming this new index as the Arid Vegetation Index: AVI). Rough scenarios of the increase in water consumption rate at the research site were generated by observing the increase in vegetated areas and collecting rough information from the farmers regarding the crop types.

Keywords: groundwater; Sentinel; Landsat; Arid Vegetation Index; El-Qaa plain; Sinai; Egypt

Citation: Morsy, M.; Michaelides, S.; Scholten, T.; Dietrich, P. Monitoring and Integrating the Changes in Vegetated Areas with the Rate of Groundwater Use in Arid Regions. *Remote Sens.* **2022**, *14*, 5767. https://doi.org/10.3390/rs14225767

Academic Editor: Raffaele Albano

Received: 9 September 2022
Accepted: 10 November 2022
Published: 15 November 2022

1. Introduction

Many arid areas are currently exhibiting a remarkable increase in socioeconomic activity [1–4]. In most of these arid areas, groundwater is the primary source of fresh water, with rainfall comprising the primary source of groundwater replenishment. Bearing in mind the scarcity of rainfall, the recharge rate of the aquifers is insufficient to compensate for the high pumping rates usually practiced by the inhabitants. In addition, the tackling of the problem becomes more difficult because many of these locations lack groundwater level measurements. Consequently, under uncontrolled pumping, groundwater resources are at risk of depletion, and these areas will rapidly degrade. The need for mitigating the

degradation effects (among others) comprises a very strong motivation to focus on devising ways to enhance the collection of groundwater measurements [5,6].

The irrigation sector in arid and semi-arid regions requires extensive pumping rates that represent 67% of the total consumption [7]. Therefore, agriculture may be used as a key parameter in the efficient framework of a groundwater management plan. Tracking the increase or decrease in the vegetated areas will provide a direct indication of the increase or decrease in the water consumption rate. Nevertheless, field measurements such as crop types, growth rates, types of irrigation, and annual expansions are not available in most arid places. In this respect, remote sensing datasets provide a good, inexpensive, and more practical alternative in an effort to develop an efficient system for tracking the annual development course of vegetation. Such an approach, however, cannot be adopted to retrieve information regarding crop types, growth rates, or types of irrigation. The selection of suitable remote sensing data plays the most important role in tracking the annual expansion of vegetated areas [8]. In order to choose the data efficiently, it is necessary, firstly, to explore the area under investigation. This may be accomplished by analyzing the geographical distribution and temporal scales of land changes, the remote sensing images spectral features, and the identification of areas that can be detected remotely [9]. It is best to compare multitemporal scenes using images obtained from the same type of sensor with the same spectral and spatial resolution and during the same seasonal time frame. This is done to ensure that there is not a significant amount of extra variation caused by a number of issues, such as solar angle, seasonal, and phenological changes [9,10]. On the one hand, because farmlands are inconsistent and unpredictable, low-resolution remote sensing data is not the ideal choice for arid regions, as it overestimates the green land parcels. Fine resolution datasets, on the other hand, constitute the best choice for such locations.

This study's goal is to track the increase or decrease in vegetated areas in locations where there are no existing reference points for vegetated land parcels. The proposed strategy may provide a proxy for tracking the increase or decrease in groundwater consumption rates. The major phases in this endeavor are (a) selecting adequate remote sensing data to track small-scale changes in vegetated regions; (b) selecting and applying relevant vegetation indices to identify land farms; (c) modifying/adapting the NDVI (Normalized Difference Vegetation Index) to better suit arid regions; and (d) developing scenarios for estimating the rate of increase or decrease in water consumption.

As an example of applying the suggested technique, the area of the city of El-Tor in Sinai, Egypt, was chosen as the research site. This location was chosen as it is an arid region on the Sinai Peninsula with significant future economic growth potential, notably in the tourist sector. These prospects have already resulted in a steady population rise and an expansion in land use. There has always been an increased demand for water in an area where groundwater is mostly drawn from the regional quaternary aquifer [6,11,12], but this demand is inflated with the increase in population and the expansion of economic activities.

For the needs of the current study, data from Landsat 7, Landsat 8, and Sentinel 2A were chosen. Five vegetation indices have been adopted: Normalized Difference Vegetation Index (NDVI), Renormalized Difference Vegetation Index (RDVI), Soil Adjuster Vegetation Index (SAVI), Enhanced Vegetation Index (EVI), and Transformed Vegetation Index (TVI). In addition, a sixth index is put forward by the authors as a modification to the NDVI, namely, the Arid Vegetation Index (AVI). Farmers at the test site were also asked to provide rough information regarding the crops they grow. Climate data from Sherief [13] was combined with the changes in vegetated areas in an attempt to provide estimates of water consumption rates at the test site. The current study is a first step for the test site in roughly determining how much water the vegetated areas consume annually, where we have no ground table measurements or idea of the volume of water used. Therefore, it could serve as a foundation for further research in this area to preserve the test site's sustainable future. Moreover, the study proposed a promising index that may perform efficiently in most arid regions.

2. Materials

2.1. Study Area

El-Tor is a small city amidst the El-Qaa plain, in the southwestern corner of the Sinai Peninsula, at 28°14′30.05″N and 33°37′19.92″E. The city is bounded by the Gulf of Suez to the west, by the Red Sea to the south, and by the Precambrian eastern mountain range to the east and north (see Figure 1). The research location is in a dry and semi-arid zone, where agricultural and built-up areas are expanding considerably. The Quaternary aquifer is the primary source of fresh groundwater at the research site [6,11,12,14–17]. It stretches from Wadi Feiran to Ras Mohamed [4,18] and is primarily refilled by rainfall [19]. Rainy events are scarce at the test site, occurring only once or twice every year. Each event occurs and lasts for several hours [6,13]. Each individual rainy event at the test site and its surroundings was categorized as light (0.1 to 1 mm), moderate (1 to 10 mm), or heavy (>10 mm) by Sherief [13]. Light rain events account for 61% of all occurrences, moderate rain events account for 34%, and heavy rain events account for 5%. These calculated percentages are based on data that Sherief collected from Egypt's Egyptian metrological authority over a 26-year period. Hence, it is very important to keep track of how much water usage is made in the research area, on a regular basis. For more details regarding the study site and its hydrological characteristics, the reader is referred to Sherief [13].

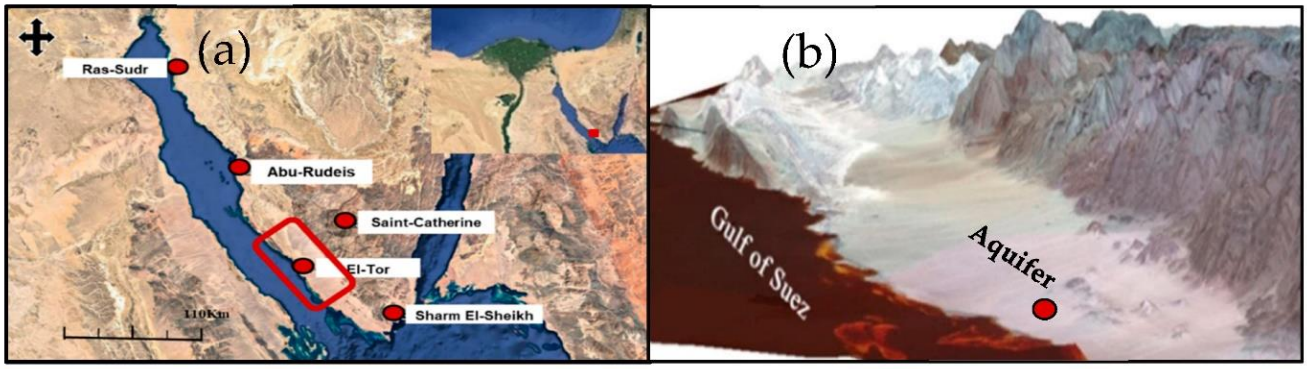

Figure 1. (**a**) Satellite map showing the research area. El-Tor city is delineated in red, and the five surrounding cities are depicted as red-filled circles that are identified (source: Google Earth, 2017) (Modified after [4]). (**b**) 3D view of the test site shows the location of the aquifer and El-Tor city (Modified after [18]).

2.2. Landsat 7 & 8

With over 40 years of data with significant resolution and over-passes, the Landsat satellites have the longest temporal record of space-based land surface measurements [20–22]. One of the most commonly used datasets for generating the NDVI index is based on data from Landsat satellites [20,23,24]. Landsat 7 was launched on 15 April 1999 [20], whereas Landsat 8 was launched on 11 February 2013 [21].

One Landsat 7 scene for each year from 2001 to 2012 for the research location were retrieved (12 scenes in total). As the satellite repeats its cycle every 16 days, the median of the available scenes per year were obtained by certain codes entered into the Google Earth engine. Landsat 8 sceneries, on the other hand, were downloaded using the same process and spanning the years from 2013 to 2021, which is nine scenes in total. All of these scenes (12 + 9) were used to track how the vegetation at the test site changed over time. The use of Landsat data is the preliminary step of the study allows us to evaluate the significance of continuing the vegetated areas expedition.

2.3. Sentinel 2A

The Sentinel 2A mission provides an unprecedented combination of systematic global coverage of land and coastal areas, a high revisit rate of five days under the same viewing conditions, high spatial resolution, and a wide field of view (295 km) for multispectral

observations from 13 bands of the electromagnetic spectrum's visible, near-infrared, and short-wave infrared ranges [22,23]. Sentinel 2A was launched on 23 June 2015 [23]. Sentinel 2A is notably useful for vegetation mapping because of the inclusion of two additional bands in the red end of the spectrum, namely at 705 and 740 nm [24]. For the purposes of this study, one scene from 2015 to 2021 with a resolution of (30 m) was retrieved for the study site (seven scenes in total). We went through the entire process again to download the same seven scenes at (10 m) resolution. Because the satellite's cycle repeats every 5 days, the median scene of the year was obtained twice (at 30 and 10 m resolution) by using appropriate Google Earth Engine codes.

2.4. Site Measurements

The available crop-related records for the test site are sparse; therefore, some information regarding the crop types and the irrigation methods was acquired by interviewing local farmers. The farmers noted the prevalence of four crops (olives, grapes, dates, and mangoes). Additionally, they stated the adoption of sprinkling irrigation at the test site. Moreover, climatic data regarding the test site, covering the period from 1979 to 2005, were obtained from Sherief [13]. The data referred to the minimum and maximum temperature, humidity, wind speed, sun hours, rain, crop type, and soil type.

2.5. Software

To achieve the study's goal, three software packages were used in tandem. The first is ArcGIS 10.5, which was used to create, calculate, and compare vegetation indices; the second is RStudio (version 1.2.1335-1), and the third software is the Cropwat 8 computer programming language that was created by the FAO's (Food and Agriculture Organization) water development division for assisting farmers in calculating the required water for their crops, based on soil, crop, and weather data [25].

3. Methods

3.1. Tracking the Increase/Decrease in Vegetated Areas

Landsat 7 and 8 (30 m) images were utilized to study the expansion of vegetated land parcels from 2001 to 2021 in order to evaluate the test site's viability for implementing the suggested concept. This preliminary step encouraged us to proceed to the next step, which was to compare the performance of Landsat data with Sentinel 2A data. Because Landsat data performs well in most arid regions [26,27], if the Sentinel 2A data is comparable, we may use it in a finer resolution to complete the rest of the procedure. This was performed by determining the increase/decrease in vegetated land parcels by calculating the NDVI of the used Sentinel 2A bands from 2015 to 2021. The correlation and differences between the used datasets were assessed. Subsequently, Sentinel 2A (10 m) was utilized to collect further information regarding the vegetated regions and to separate agricultural parcels from the land area. The extraction of these parcels allowed us to avoid camouflage with the surrounding colorful lithology, allowing for improved tracking of vegetated parcels. The Google Earth Engine downloaded all the required datasets. ArcGIS 10.5 was utilized to compute the NDVI as well as to track and extract agricultural parcels (Figure 2). Using RStudio, the correlation between the datasets was calculated.

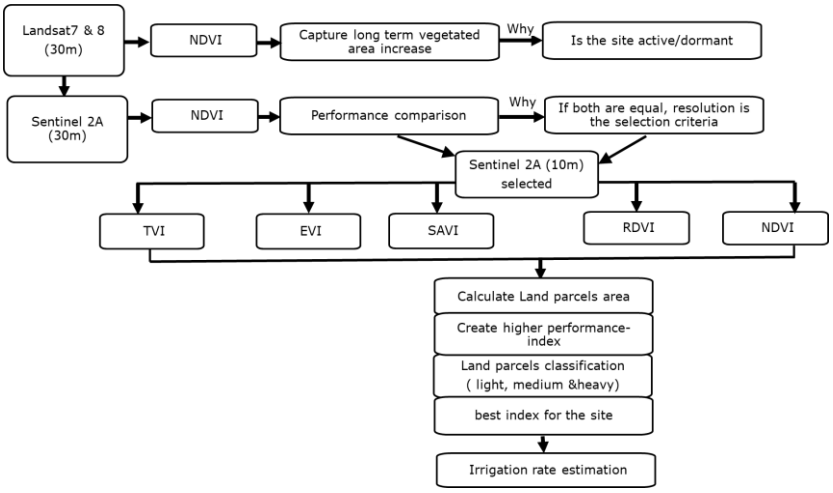

Figure 2. The used technique and data to roughly estimate the irrigation rate at the study site.

3.2. Testing Different Vegetation Indices

Vegetation indices were evaluated on Sentinel 2A (10 m) data to track and categorize vegetated parcels as heavy, moderate, and sparse from 2015 to 2021; the indices used are the NDVI [28], RDVI [29], SAVI [30], EVI [31], and TVI [32], as described mathematically in Equations (1) to (5):

$$\mathrm{NDVI} = (\mathrm{NIR} - \mathrm{red})/(\mathrm{NIR} + \mathrm{red}) \quad (1)$$

$$\mathrm{RDVI} = (\mathrm{NIR} - \mathrm{red})/\sqrt{(\mathrm{NIR} + \mathrm{red})} \quad (2)$$

$$\mathrm{SAVI} = (1 + \mathrm{L})(\mathrm{NIR} - \mathrm{Red})/(\mathrm{NIR} + \mathrm{Red} + \mathrm{L}) \quad (3)$$

$$\mathrm{EVI} = 2.5 \times \frac{(\mathrm{NIR} - \mathrm{Red})}{(\mathrm{NIR} + 6 \times \mathrm{Red} - 7.5 \times \mathrm{Blue} + 1)} \quad (4)$$

$$\mathrm{TVI} = \sqrt{(\mathrm{NIR} - \mathrm{Red})/(\mathrm{NIR} + \mathrm{Red}) + 0.5} \quad (5)$$

To obtain the optimum performance of the suggested concept, it is essential to select the index with the highest performance at the test site. From 2015 to 2021, the correlation and differences between all of the above indices, which include light, medium, and heavy vegetation, have been calculated.

3.3. The Arid Vegetation Index (AVI)

At first, the performance of the above five indices was evaluated, but it became evident that a higher-performing index was required. In this respect, the NDVI index was adjusted by developing a more appropriate version for arid places with sparse vegetation. The new index is the Arid Vegetation Index (denoted hereafter as AVI), which was conceptualized in an effort to enhance the contrast between adjacent pixels:

$$\mathrm{AVI} = [(\mathrm{NIR} - \mathrm{Red})/(\mathrm{NIR} + \mathrm{Red})] \times \mathrm{VNIR} \quad (6)$$

NDVI measures the difference between near-infrared (which vegetation strongly reflects) and red light (which vegetation absorbs) to quantify vegetation. Near-infrared (B6 or VNIR) is one of the bands designated for vegetation detection; chlorophyll reflects this band particularly well. Therefore, in an infrared image, denser vegetation appears as red and urban areas as white. By multiplying the NDVI index by Band 6 (B6) in the Sentinel 2A data, it may be possible to increase the contrast between adjacent pixels. The proposed index was evaluated using the accuracy evaluation approach by adding 30 points to the 2021 Sentinel 2A (10 m) AVI image and comparing the correctness of the indices with the placement of the points on the 2022 Google Earth image. At the test site, thirty points

were placed onto a single farm that had all four-pixel values (light vegetation, moderate vegetation, heavy vegetation, and bare soil) (Figure 3).

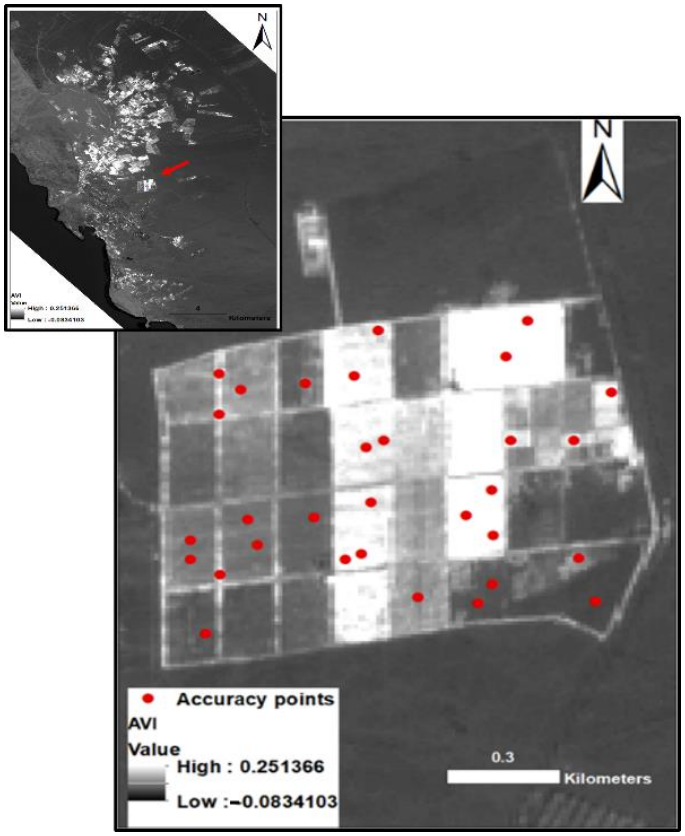

Figure 3. The AVI resulted from the use of the Sentinel 2A (10 m) bands. It shows the accuracy and the high resolution of the data. The accuracy assessment test was applied on one farm containing all the vegetation classes (heavy, moderate, and light). The position of the farm is shown by the red arrow.

3.4. Crop Consumption Rate Measurements

The site's irrigation rate was calculated using three sources of data. Grapes, mangoes, dates, and olives were among the crops that farmers brought in for the first batch. The second set is based on data from Sherief [13] and includes climatological variables such as minimum and maximum temperatures, rainfall, humidity, wind speed, and the number of hours of sunshine each day. The last set is based on crop and soil parameters that are built into the used software. Using all the information gathered, the Cropwat 8 software was able to determine how much water each crop variety consumed [33] (Figure 4). Cropwat 8 computes the irrigation rate for each crop type by considering sprinkling irrigation, by default. Each crop type's mean monthly reference evapotranspiration (ETo) was calculated using the Penman–Monteith equation [34], and the effective rainfall (EFF) represents the amount of precipitation that is utilized by the plants. Finally, crop and soil parameters such as crop coefficient, root length, ponding depth, transplanting date, and harvest date were collected and used in the calculation of the irrigation rate. When there is a scarcity of field measurements, Cropwat 8 has a pre-recorded database for each crop variety that may be used instead. The increase or decrease in vegetative areas, which was registered by AVI, was combined with the irrigation rate to determine how much more or less water was used.

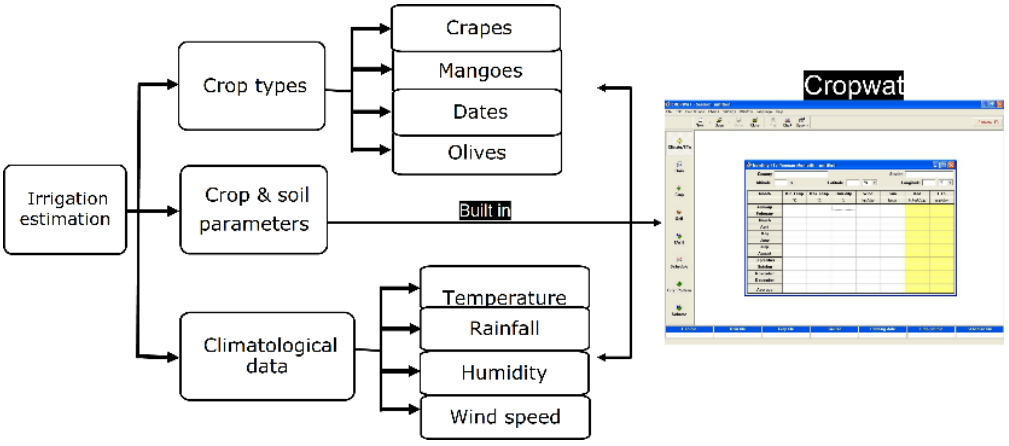

Figure 4. The datasets used to calculate the consumption rate of each crop type by Cropwat 8.

4. Results

4.1. Tracking Increase/Decrease in Vegetated Areas

The tracking of vegetated areas using Landsat 7 and 8 data revealed a significant increase in vegetated land parcels from 2001 to 2021 (Figure 5). The land-farm area calculated using the NDVI index on Landsat 7 bands in 2001 was 2.9 km^2. Landsat 8 data showed that this gradually increased to 23.3 km^2 by 2021 (Figure 5). This step is followed by a comparison between the NDVI of Landsat 8 and Sentinel 2A data recorded between 2015 and 2021. The NDVI on Landsat 8 in 2015 recorded 9 km^2 of vegetated areas; however, 23.3 km^2 was determined in 2021. The NDVI on the Sentinel data, on the other hand, recorded 7.6 km^2 in 2015 and 21.7 km^2 in 2021. Both datasets showed a strong correlation during the period 2015 to 2021, with R = 0.85 (Figure 6). These results confirmed that the use of finer resolution data will be vital for the completion of the proposed target.

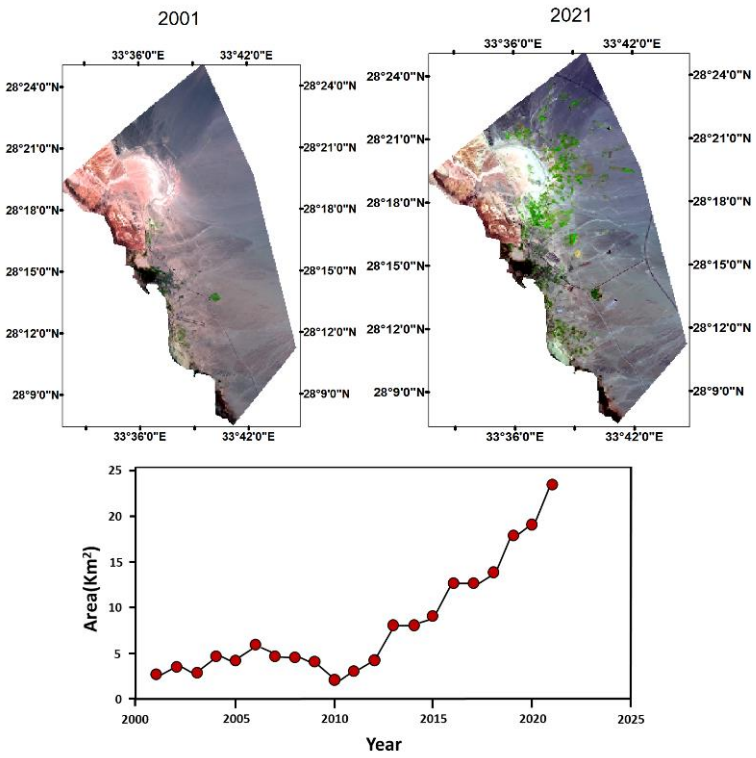

Figure 5. The upper part of the figure shows the increase in vegetated area from 2001 to 2021, captured by two Landsat 7 and 8 scenes. The lower part displays the gradual increase in the vegetated areas from 2001 to 2021, as captured by the NDVI index that is applied to Landsat 7 and 8 bands.

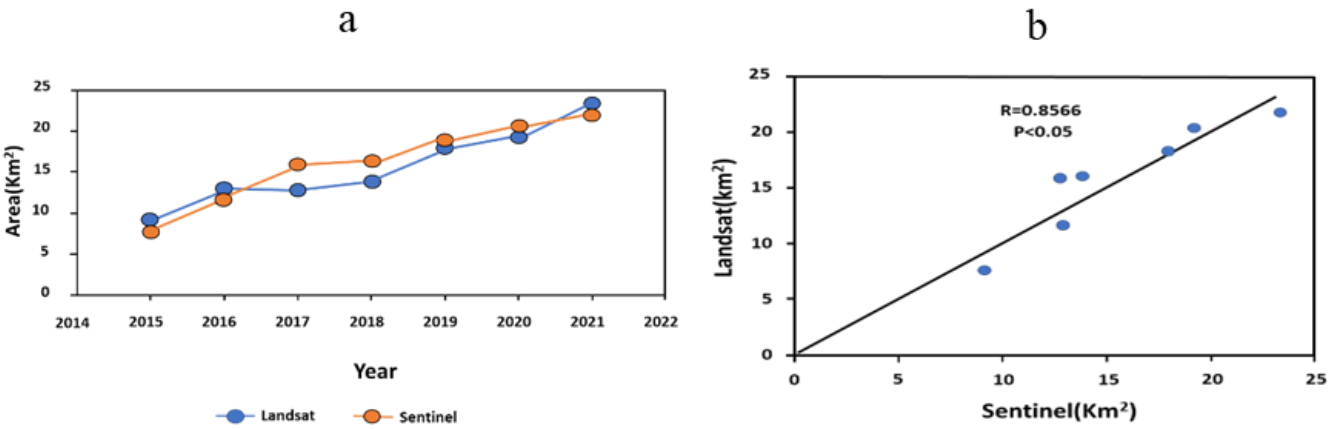

Figure 6. (**a**) The increase in the vegetated areas detected by Landsat 8 and Sentinel 2A data during the period from 2015 to 2021; (**b**) The correlation between remote sensing datasets (based on NDVI index).

4.2. Testing Different Vegetation Indices

Sentinel 2A (10 m) was used to determine the vegetated areas using the indices NDVI, RDVI, SAVI, EVI, and TVI. NDVI typically range from −1.0 to +1.0, with higher positive values suggesting denser and/or healthier vegetation [35]. However, at the test site, pixels ranging from 0.7 to 0.4 were classified as heavy vegetation and recorded 0.8 km^2 in 2015 and 1.9 km^2 in 2021; pixels ranging from 0.4 to 0.2 were classified as moderate vegetation and recorded 2.3 km^2 in 2015 and 5.5 km^2 in 2021; and pixels ranging from 0.2 to 0.09 were classified as light vegetation and recorded 5.4 km^2 in 2015 and 11.9 km^2 in 2021. In all, 8.6 km^2 were recorded in 2015, with 19.4 km^2 recorded in 2021. The RDVI index at the test location reported 0.77 km^2 of vegetated areas in 2015 and 1.98 km^2 in 2021, with pixel values ranging from 0.5 to 0.24 being classified as heavy vegetation. Those ranging from 0.24 to 0.16 are classified as moderate vegetation and cover an area ranging from 1.9km^2 in 2015 to 4.7 km^2 in 2021, while those ranging from 0.16 to 0.09 are categorized as light vegetation, with 4.1 km^2 reported in 2015 and 8.7 km^2 in 2021.

The SAVI index yielded 6.9 km^2 in 2015 and 15.5 km^2 in 2021. In 2015 and 2021, thick vegetation pixels varied in value from 0.54 to 0.26, recording 0.74 km^2 to 1.93 km^2. In 2015 and 2021, the value of moderate vegetation pixels ranged from 0.26 to 0.17, with 1.96 km^2 to 4.73 km^2. The bright vegetation pixels had values ranging from 0.17 to 0.1 and covered an area ranging from 4 km^2 to 8.3 km^2. In 2015, there were 6.7 km^2, and by 2021 there were 15.0km^2. Heavy vegetation pixels varied in value from 0.8 to 0.3 for the EVI index, with 0.7 km^2 and 1.8 km^2 reported in 2015 and 2021, respectively. The pixel values of the moderate vegetation varied from 0.3 to 0.1, with 2.3 km^2 recorded in 2015 and 5.7 km^2 recorded in 2021. While light pixel values ranged from 0.1 to 0.09, 5.6 km^2 was measured in 2015 and 12.7 km^2 in 2021. The TVI index values for heavy vegetation range from 1 to 0.7, moderate vegetation ranges from 0.7 to 0.6, and light vegetation ranges from 0.6 to 0.5. Heavy vegetation had pixel values of 1 km^2 in 2015 and 2.3 km^2 in 2021, whereas moderate vegetation had pixel values of 2.7 km^2 in 2015 and 6.4 km^2 in 2021. Heavy vegetation pixels reported 5.8 km^2 in 2015 and 13.4 km^2 in 2021. The Pearson correlation between the five indices was computed. All the indices utilized were strongly correlated with one another, with an R = 0.9 and a $p < 0.05$ in all (Figure 7).

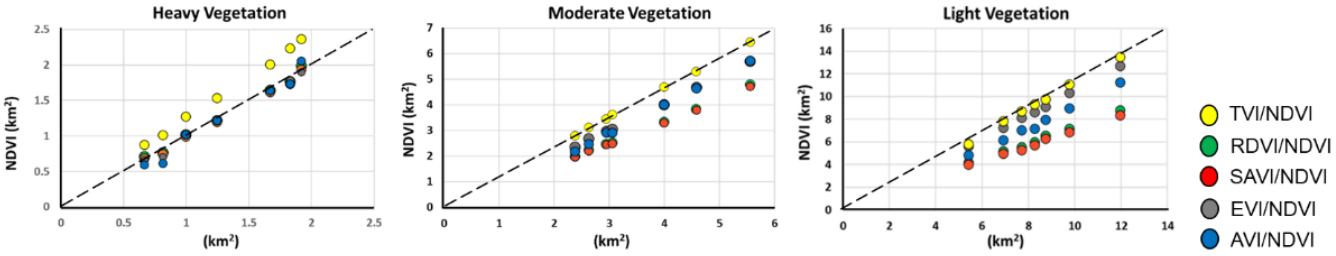

Figure 7. The correlation between the NDVI and all the used indices for the heavy, moderate, and light vegetation.

4.3. Testing the Accuracy of AVI

The proposed index, namely AVI, showed the best performance compared to the other indices. The accuracy percentage of the AVI index is 96.6% at the test site, while the accuracy of the NDVI is 83.3% (Table 1). The AVI index exhibited better resolution, even when zooming in to the Sentinel image. The index showed clear pixels and was easy to differentiate at the study site.

Table 1. Accuracy assessment of all the used vegetation indices.

Index	NDVI	SAVI	EVI	RDVI	TVI	AVI
Accuracy	83.3%	66.6%	86.6%	76.6%	80%	96.6%

4.4. Crop Consumption Rate Measurements

Cropwat 8 revealed the irrigation rate of each crop type at the beginning, middle, and end of the growing period. The mean of the three stages of the four crop types was calculated. Grapes consume 642.6 mm/ha at the test location, mangoes require 1304.1 mm/ha, dates use 1218.6 mm/ha, and olives consume 785.1 mm/ha (Figure 8 and Table 2). By using this data, we were able to merge the consumption rate per hectare with the increase in vegetated areas recorded by the Sentinel 2A data and the AVI index. To effectively complete this stage, several irrigation scenarios for the test site were assumed, the first of which is that grapes occupy 50% of the test site, mangoes occupy 20%, and dates and olives each occupy 15% of the test site. The second scenario has olives taking up half of the space, dates taking up 20%, and mangoes and grapes taking up 15%. In the third scenario, mangoes take up half of the third space, olives take up 20%, while grapes and dates take up 15%. The fourth is dominated by dates, with 15% olives, 15% mangos, and 25% grapes. The fifth scenario calls for 25% coverage by each crop (Figure 8). To complete the procedure, the needed irrigation units were converted to m^3/year and, subsequently, to m^3/hour. The conversion was based on Saravanan and Saravanan [36], who noted that the Cropwat 8 measuring unit is expressed in mm/ha per year and that 1 mm = 10 m^3/ha. Based on the information provided, the units were adjusted from m^3/year to m^3/h. The first scenario suggested a progressive rise in irrigation rates, with 866.495 m^3/h in 2015 and 1956.135 m^3/h in 2021. The second scenario measured 908.145 m^3/h in 2015 and 2050.16 m^3/h in 2021. In 2015, the third scenario yielded 1089.9 m^3/h and 2460.425 m^3/h. In the fourth scenario, water consumption grew from 883.19 m^3/h in 2015 to 1993.795 m^3/h to 2021. The fifth one increased from 969.7 m^3/h in 2015 to 2189.1 m^3/h in 2021 (see Figure 9).

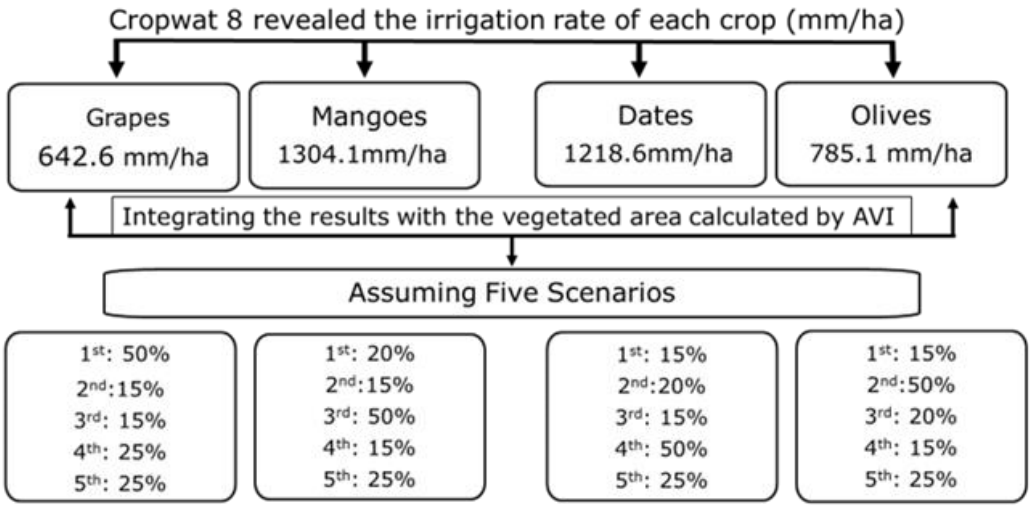

Figure 8. The results of the analysis with Cropwat 8 and the proposed scenarios.

Table 2. The effective rain (EFF), potential crop evapotranspiration (ETC), and irrigation required (IR), for each crop type.

		EFF (mm)	ETC (mm)	IR (mm)
Group	Grapes	7.9	655.6	642.6
	Mangoes	7.9	1322.6	1304.1
	Dates	7.9	1237.5	1218.6
	Olives	3.8	789	785.1

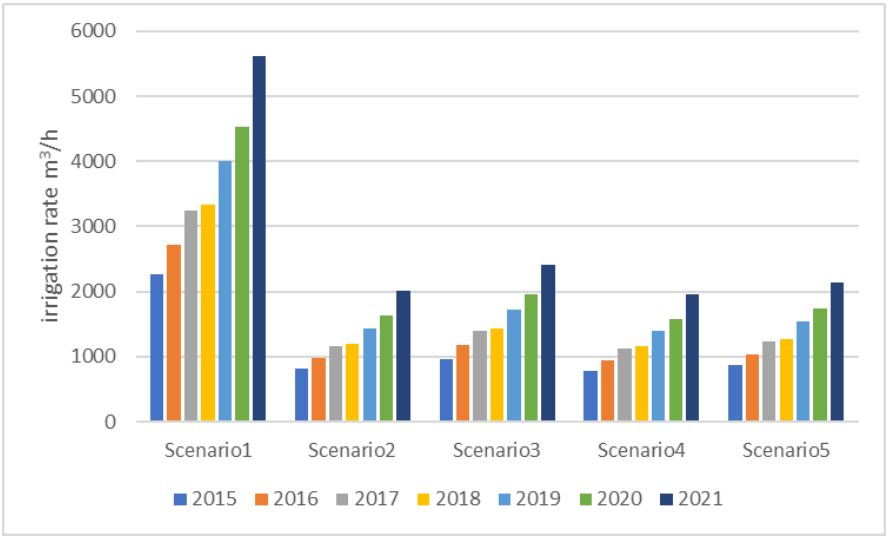

Figure 9. The consumption rate recorded by each proposed scenario.

5. Discussion

In this study, the focus is on estimating groundwater availability, which is of crucial importance in areas where this is a major source of freshwater. An understanding of the spatiotemporal characteristics of hydrological components, such as the level of groundwater, is critical for comprehending the underlying complex hydrological, climatological, and ecological processes and attending effective water management challenges [37]. Approximately one-third of the Earth's land surface is categorized as hyper-arid, semi-arid, or arid; regions with arid environments are inhabited by over 38% of the world's population [38]. Generally, plant diversity in such environments is relatively low and vegetation cover is

generally sparse, but it may be enhanced in the areas where groundwater is available. However, where unsustainable extraction of groundwater is practiced, groundwater-dependent ecosystems are under increased threat. Under such conditions, proper monitoring of groundwater availability is a vital component of a water management system.

In a study carried out by Halipu et al. [39] in a hyper-arid region in Egypt, the authors quantified the water consumption using two different approaches: one based on land use/land cover by using optical remote sensing data, and the other based on groundwater storage changes with the use of satellite data (from the Gravity Recovery Climate Experiment). It is worth mentioning that there are similarities in the profiles of the area used in the present study and that used by the above authors: the primary water consumption sector is agriculture because agricultural land consumes more than 90% of the available water resources; the population has also notably increased. Both approaches adopted by Halipu et al. [39] in New Valley showed an increase in irrigation water usage and a continuous decrease in the groundwater storage over the area of study. The overall domestic and irrigation water usage in New Valley was calculated as 18.62 km^3 based on the LULC estimates; the groundwater storage changes of New Valley based on the satellite data were calculated to be 19.36 ± 7.96 km^3. These findings indicated a consistency between the results of the two approaches.

Wei et al. [40] used various remote sensing products, climate data, and ancillary information to estimate irrigation rate with the use of machine learning techniques. The authors were able to capture the temporal and spatial variability of irrigation amounts with a satisfactory accuracy. The difference between the mentioned studies and ours is the availability of in situ measurements of climate, crop types, growth stage, irrigation pace, and growth stage.

In arid areas, a key element in water management is the monitoring of the rise and fall of the water table level. However, in most dry environments, no in situ measurements are available to aid in tracking the ground water levels. Tracking the increase or decrease in vegetated areas may provide an alternative, as in these regions most of the water is consumed for irrigation purposes. Due to a lack of field measurements and accessibility issues, in this study, remote sensing data were employed to showcase the proposed method, by applying it to the research site chosen. One of the most critical steps was the collection of data that were appropriate for the research site. The data from MODIS and AVHRR were insufficient for the El-tor because of their coarse resolution. These data overestimated the vegetated regions, and they did not perform adequately with sparsely dispersed vegetated areas. However, because of their relatively fine resolution, Landsat and Sentinel data performed well for the test site. Landsat 7 and 8 (30 m) data indicated a considerable rise in vegetated regions from 2001 to 2021; Sentinel 2A (30 m) data, on the other hand, showed a noticeable increased efficiency from 2015 to 2021 because the mission began in 2015. Sentinel 2A (10 m) was able to distinguish between densely vegetated, moderately vegetated, and sparsely vegetated land parcels. Furthermore, five vegetation indicators were evaluated in order to identify the best one for the test location. However, we investigated the connection between each of the two indices, and the correlation was quite strong in all of them, with R values of 0.9.

Furthermore, the NDVI was modified to better fit dry locations by multiplying the NDVI index by VNIR; this has yielded clearer findings at our test site (Figure 10). In addition, the accuracy evaluation approach was used to ensure that the proposed AVI formula performs better for the research location. The accuracy rating is based on the classification of a farm into thick, moderate, and sparse vegetation, with a total of 30 points. There were some noticeable differences between the modified formula of the arid regions (AVI) and the rest of the indices, as it showed the highest contrast between the neighboring cells.

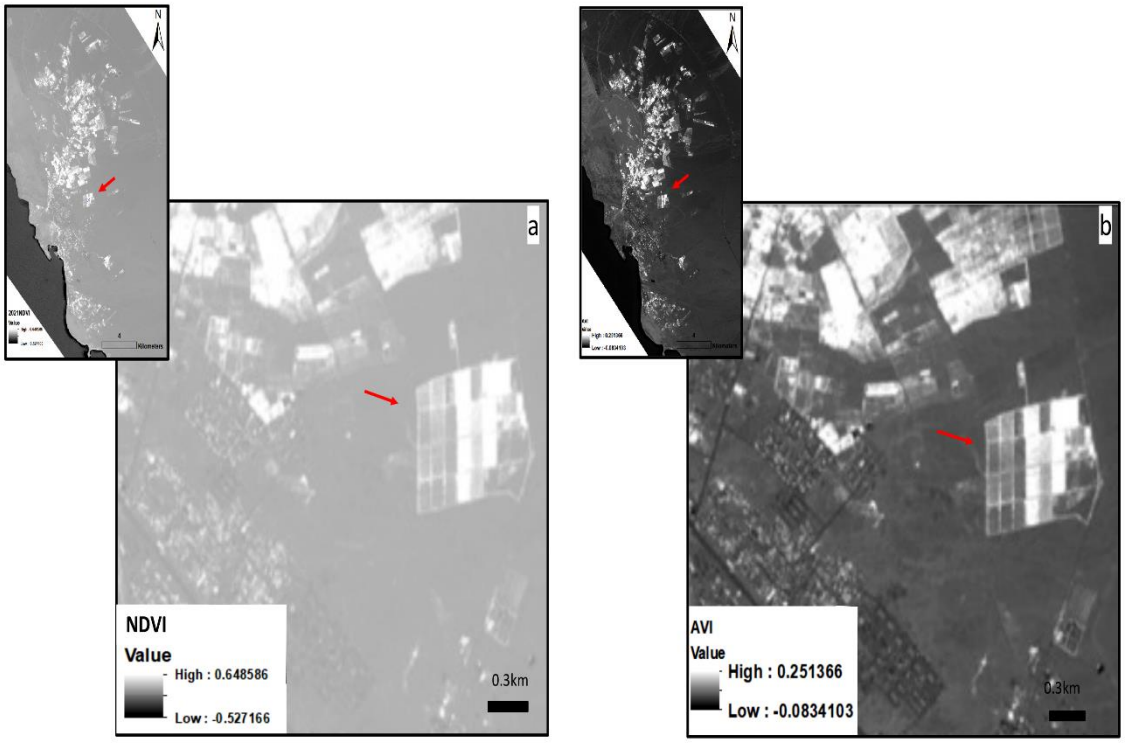

Figure 10. The difference between (**a**) NDVI and (**b**) AVI indices by applying both on Sentinel 2A data for 2021. The red arrow shows the farm that contains light, moderate, and heavy vegetation.

Because the AVI performed the best at the test site, it was subsequently used with climate data from Sherief (2008) and field data acquired from farmers on crop types and irrigation techniques. All of the data stated above were utilized in Cropwat 8 to generate scenarios for the irrigation at the test site. This stage revealed that the research site's water consumption fluctuated between 785 m^3/h and 2256 m^3/h in 2015 and from 1954 m^3/h to 5618 m^3/h in 2021, indicating an increase of more than 100% in just six years.

The inferred rise in the water consumption rate, as a result of the presented scenarios, revealed that the dominant aquifer is under stress and that the habits of the residents may result in negative repercussions that threaten the future of the study site and impede extension plans.

Bearing in mind that in the study area no groundwater measurements are obtainable, the proposed methodology has the advantage that it can be adopted in areas where no in situ measurements are available, but it makes use of remote sensing data that are available in sufficient spatiotemporal resolutions. The major benefit stemming from this study lies in the fact that in areas with insufficient data, even a rough assessment of the groundwater conditions could provide a timely alarm, especially where there is a high risk of detrimental saltwater intrusion into coastal aquifers due to excessive pumping [41]. Such a timely warning could trigger effective mitigation measures that are vital for the sustainability of freshwater aquifers.

The lack of groundwater monitoring records, even on a regional basis, is a common issue in many parts of the world that hampers a sufficient understanding of the hydrological conditions and the efficient management of water resources. For example, in the study in the river Nile basin by Nigatu et al. [42], the limitations in obtaining groundwater data over the region are ascribed to the cross-country boundary location of the basin and the lack of political will by the respective countries to share data. Nevertheless, whatever the reason for lacking sufficient groundwater measurements, the impact is on ineffective water management practice and subsequently diminishing food production and an increase in the threat of food insecurity. In the same study, Nigatu et al. [42] underscore the use of

satellite data sources sets as a proxy to efficiently and affordably monitoring groundwater availability and obtain a broader picture at the basin scale.

The Sentinel mission offers 12 bands, each with a different resolution. At the start of the mission, the authors expended considerable effort in resampling the layers. However, GEE devised a solution and gave all users free access to Sentinel bands with the same resolution by selecting the appropriate code. Using 10 m resolution bands allows you to see more details in sites with sparse vegetation. However, coarse resolution datasets such as MODIS and AVHRR overestimated the vegetated areas at our site and did not work for the case study. These datasets, however, may work well in larger areas with dense vegetation.

6. Concluding Remarks

This study represents a contribution towards a better understanding of groundwater's long-term sustainability in the effort to establish appropriate policies for decision-makers [42] with regard to a more efficient water sources management. This paper presents an integrated technique as well as a new index to proxy estimates of the changes in water consumption rates in arid areas; these estimates can aid in the planning of a more efficient water management scheme. The proposed method is based on tracking the increase or decrease in vegetated areas, which indicates an increase and decrease of 65 percent of water used in dry regions. The approach is based on remote sensing data from high-resolution Landsat and Sentinel satellites. Furthermore, the study verified the effectiveness of the modified index (AVI) in dry regions when combined with Sentinel 2A data. We were able to trace the range consumption by vegetated areas at the research location for the previous 7 years by employing both and collecting minimum in situ data. Furthermore, taking more in-person reports of crop types and growth rates will help to ensure the data are correct.

Several precautions must be taken at the test site to prevent the potential future repercussions of the high pumping rates. First, it is important raise water conservation awareness among residents and farmers. This might be accomplished by converting from sprinkler irrigation to drip irrigation. In addition, the prohibition on farmers drilling random wells will further preserve groundwater. Citizens should also help gather ongoing measurements of the water table and record the number of wells that have dried up. In such areas, the engagement of stakeholders and the government is crucial.

It is not possible to calculate absolute values of irrigation rates within the framework of the proposed methodology due to a lack of in situ measurements on climatic variables, phenological properties of crops, and the exact areal extension of each crop and its exact location at the test site. Furthermore, if the farmers provided inaccurate information regarding the crop types, this will have an impact on the irrigation rate calculated for each year. All of these challenges were encountered in this current work, as a result of the difficulties in having physical access to the test site and due to lack of in situ data.

On a local scale, the article is a first step toward protecting the aquifer from depletion. Furthermore, it demonstrates that farmers are using some incorrect practices, such as selecting crop types that require a high irrigation rate and a high pumping rate. Furthermore, it may focus the attention of stakeholders on spreading awareness among farmers and developing strict plans to preserve the test site's sustainable future. On a regional scale, the study provides a new index that will be useful to Sentinel mission users, particularly those working in arid regions.

There can be no better substitute to the actual well-planned and well-structured measurements. However, in the absence of such in situ records, the present paper proposes a methodology that can be considered as a first step in a region characterized by extremely sparse climatic archives, no field measurements on the water table level, no documented records of crop types, non-existent information on irrigation rates, and no evidence of phenological properties.

Author Contributions: Conceptualization, M.M. and P.D.; software, M.M.; validation, M.M. and S.M.; formal analysis, M.M., P.D. and T.S.; investigation, M.M. and S.M.; resources, P.D.; data curation, M.M. and T.S.; original draft preparation, M.M; writing—review and editing, M.M. and S.M.; visualization M.M. and T.S.; supervision P.D. and T.S.; project administration, P.D.; funding acquisition, P.D. All authors have read and agreed to the published version of the manuscript.

Funding: This work was supported by the Helmholtz Center for Environmental Research in Leipzig, Germany, UFZ.

Data Availability Statement: The remote sensing data were downloaded from Google Earth Engine (https://code.earthengine.google.com/ (accessed on 11 November 2022)) and the climatological data were retrieved from the study by Sherief [13].

Acknowledgments: Mona Morsy is supported by Helmholtz Center for Environmental Research in Leipzig, Germany, UFZ. Silas Michaelides is supported by the "EXCELSIOR: ERATOSTHENES: Excellence Research Centre for Earth Surveillance and Space-Based Monitoring of the Environment" H2020 Widespread Teaming project (www.excelsior2020.eu (accessed on 11 November 2022)), which has received funding from the European Union's Horizon 2020 research and innovation programme under Grant Agreement No 857510, from the Government of the Republic of Cyprus through the Directorate General for the European Programmes, Coordination and Development, and the Cyprus University of Technology. The authors appreciate the comments made by three anonymous reviewers and wish to thank them for their constructive suggestions.

Conflicts of Interest: The authors declare no conflict of interest.

References

1. Dregne, H.; Kassas, M.; Rozanov, B. A New Assessment of the World Status of Desertification. *Desertif. Control Bull.* **1991**, *20*, 6–29.
2. Scanlon, B.R.; Keese, K.E.; Flint, A.L.; Flint, L.E.; Gaye, C.B.; Edmunds, W.M.; Simmers, I. Global Synthesis of Groundwater Recharge in Semiarid and Arid Regions. *Hydrol. Process.* **2006**, *20*, 3335–3370. [CrossRef]
3. Yin, L.; Zhang, E.; Wang, X.; Wenninger, J.; Dong, J.; Guo, L.; Huang, J. A GIS-Based DRASTIC Model for Assessing Groundwater Vulnerability in the Ordos Plateau, China. *Environ. Earth Sci.* **2013**, *69*, 171–185. [CrossRef]
4. Morsy, M.; Scholten, T.; Michaelides, S.; Borg, E.; Sherief, Y.; Dietrich, P. Comparative Analysis of TMPA and IMERG Precipitation Datasets in the Arid Environment of El-Qaa Plain, Sinai. *Remote Sens.* **2021**, *13*, 588. [CrossRef]
5. Sheffield, J.; Wood, E.F.; Pan, M.; Beck, H.; Coccia, G.; Serrat-Capdevila, A.; Verbist, K. Satellite Remote Sensing for Water Resources Management: Potential for Supporting Sustainable Development in Data-Poor Regions. *Water Resour. Res.* **2018**, *54*, 9724–9758. [CrossRef]
6. Morsy, M.; Taghizadeh-Mehrjardi, R.; Michaelides, S.; Scholten, T.; Dietrich, P.; Schmidt, K. Optimization of Rain Gauge Networks for Arid Regions Based on Remote Sensing Data. *Remote Sens.* **2021**, *13*, 4243. [CrossRef]
7. Makhamreh, Z.; Hdoush, A.A.A.; Ziadat, F.; Kakish, S. Detection of Seasonal Land Use Pattern and Irrigated Crops in Drylands Using Multi-Temporal Sentinel Images. *Environ. Earth Sci.* **2022**, *81*, 120. [CrossRef]
8. Weber, C.; Puissant, A. Urbanization Pressure and Modeling of Urban Growth: Example of the Tunis Metropolitan Area. *Remote Sens. Environ.* **2003**, *86*, 341–352. [CrossRef]
9. Li, H.; Zheng, L.; Lei, Y.; Li, C.; Liu, Z.; Zhang, S. Estimation of Water Consumption and Crop Water Productivity of Winter Wheat in North China Plain Using Remote Sensing Technology. *Agric. Water Manag.* **2008**, *95*, 1271–1278. [CrossRef]
10. Coppin, P.R.; Bauer, M.E. Digital Change Detection in Forest Ecosystems with Remote Sensing Imagery. *Remote Sens. Rev.* **1996**, *13*, 207–234. [CrossRef]
11. Adhikary, P.P.; Chandrasekharan, H.; Dubey, S.K.; Trivedi, S.M.; Dash, C.J. Electrical Resistivity Tomography for Assessment of Groundwater Salinity in West Delhi, India. *Arab. J. Geosci.* **2015**, *8*, 2687–2698. [CrossRef]
12. Elavarasi, S.A.; Akilandeswari, J.; Sathiyabhama, B. A Survey on Partition Clustering Algorithms. Available online: http://www.ijecbs.com/January2011/N6Jan2011.pdf (accessed on 21 August 2021).
13. Sherief, Y. Flash Floods and Their Effects on the Development in El-Qaá Plain Area in South Sinai, Egypt, a Study in Applied Geomorphology Using GIS and Remote Sensing. Available online: https://openscience.ub.uni-mainz.de/handle/20.500.12030/2211 (accessed on 11 November 2022).
14. EL-Refai, A.A. *Water Resources of Southern Sinai, Egypt*; Geomorphological and Hydrogeological Studies; University of Cairo: Giza, Egypt, 1992.
15. El-Fakharany, M.A. Geophysical and Hydrogeochemical Investigations of the Quaternary Aquifer at the Middle Part of El Qaa-Plain SW Sinai, Egypt. *Egypt. J. Geol.* **2016**, *47*, 1003–1022.
16. Ahmed, M.; Sauck, W.; Sultan, M.; Yan, E.; Soliman, F.; Rashed, M. Geophysical Constraints on the Hydrogeologic and Structural Settings of the Gulf of Suez Rift-Related Basins: Case Study from the El Qaa Plain, Sinai, Egypt. *Surv. Geophys.* **2014**, *35*, 415–430. [CrossRef]

17. Rashed, M.; Sauck, W.; Soliman, F. Gravity, Magnetic, and Geoelectric Survey on EL-Qaa Plain, Southwest Sinai, Egypt. In Proceedings of the 8th Conference Geology of Sinai for Development, Ismailia, Egypt, 3 December 2007; pp. 15–20.
18. Wahid, A.; Madden, M.; Khalaf, F.; Fathy, I. Geospatial Analysis for the Determination of Hydro-Morphological Characteristics and Assessment of Flash Flood Potentiality in Arid Coastal Plains: A Case in Southwestern Sinai, Egypt. *Earth Sci. Res. J.* **2016**, *20*, E1–E9. [CrossRef]
19. Massoud, U.; Santos, F.; El Qady, G.; Atya, M.; Soliman, M. Identification of the Shallow Subsurface Succession and Investigation of the Seawater Invasion to the Quaternary Aquifer at the Northern Part of El Qaa Plain, Southern Sinai, Egypt by Transient Electromagnetic Data. *Geophys. Prospect.* **2010**, *58*, 267–277. [CrossRef]
20. Goward, S.N.; Masek, J.G.; Williams, D.L.; Irons, J.R.; Thompson, R.J. The Landsat 7 Mission: Terrestrial Research and Applications for the 21st Century. *Remote Sens. Environ.* **2001**, *78*, 3–12. [CrossRef]
21. Irons, J.R.; Dwyer, J.L.; Barsi, J.A. The next Landsat Satellite: The Landsat Data Continuity Mission. *Remote Sens. Environ.* **2012**, *122*, 11–21. [CrossRef]
22. Drusch, M.; Del Bello, U.; Carlier, S.; Colin, O.; Fernandez, V.; Gascon, F.; Hoersch, B.; Isola, C.; Laberinti, P.; Martimort, P.; et al. Sentinel-2: ESA's Optical High-Resolution Mission for GMES Operational Services. *Remote Sens. Environ.* **2012**, *120*, 25–36. [CrossRef]
23. Gascon, F.; Bouzinac, C.; Thépaut, O.; Jung, M.; Francesconi, B.; Louis, J.; Lonjou, V.; Lafrance, B.; Massera, S.; Gaudel-Vacaresse, A.; et al. Copernicus Sentinel-2A Calibration and Products Validation Status. *Remote Sens.* **2017**, *9*, 584. [CrossRef]
24. Clerici, N.; Valbuena Calderón, C.A.; Posada, J.M. Fusion of Sentinel-1a and Sentinel-2A Data for Land Cover Mapping: A Case Study in the Lower Magdalena Region, Colombia. *J. Maps* **2017**, *13*, 718–726. [CrossRef]
25. Shekhar, S.; Kumar, S.; Sinha, R.; Gupta, S.; Densmore, A.; Rai, S.P.; Kumar, M.; Singh, A.; Van Dijk, W.; Joshi, S.; et al. Efficient Conjunctive Use of Surface and Groundwater Can Prevent Seasonal Death of Non-Glacial Linked Rivers in Groundwater Stressed Areas. In *Clean and Sustainable Groundwater in India*; Springer: Singapore, 2018; pp. 117–124. [CrossRef]
26. Jia, K.; Li, Y.; Liang, S.; Wei, X.; Yao, Y. Combining Estimation of Green Vegetation Fraction in an Arid Region from Landsat 7 ETM+ Data. *Remote Sens.* **2017**, *9*, 1121. [CrossRef]
27. Nutini, F.; Boschetti, M.; Brivio, P.A.; Bocchi, S.; Antoninetti, M. Land-Use and Land-Cover Change Detection in a Semi-Arid Area of Niger Using Multi-Temporal Analysis of Landsat Images. *Int. J. Remote Sens.* **2013**, *34*, 4769–4790. [CrossRef]
28. Pettorelli, N.; Vik, J.O.; Mysterud, A.; Gaillard, J.M.; Tucker, C.J.; Stenseth, N.C. Using the Satellite-Derived NDVI to Assess Ecological Responses to Environmental Change. *Trends Ecol. Evol.* **2005**, *20*, 503–510. [CrossRef] [PubMed]
29. Chen, J.M. Evaluation of Vegetation Indices and a Modified Simple Ratio for Boreal Applications. *Can. J. Remote Sens.* **1996**, *22*, 229–242. [CrossRef]
30. Huete, A.R. A Soil-Adjusted Vegetation Index (SAVI). *Remote Sens. Environ.* **1988**, *25*, 295–309. [CrossRef]
31. Huete, A.; Didan, K.; Miura, T.; Rodriguez, E.P.; Gao, X.; Ferreira, L.G. Overview of the Radiometric and Biophysical Performance of the MODIS Vegetation Indices. *Remote Sens. Environ.* **2002**, *83*, 195–213. [CrossRef]
32. Mutanga, O.; Skidmore, A.K. Narrow Band Vegetation Indices Overcome the Saturation Problem in Biomass Estimation. *Int. J. Remote Sens.* **2004**, *25*, 3999–4014. [CrossRef]
33. Tan, M.; Zheng, L. Different Irrigationwater Requirements of Seed Corn and Field Corn in the Heihe River Basin. *Water* **2017**, *9*, 606. [CrossRef]
34. Allen, R.G.; Pruitt, W.O.; Wright, J.L.; Howell, T.A.; Ventura, F.; Snyder, R.; Itenfisu, D.; Steduto, P.; Berengena, J.; Yrisarry, J.B.; et al. A Recommendation on Standardized Surface Resistance for Hourly Calculation of Reference ETo by the FAO56 Penman-Monteith Method. *Agric. Water Manag.* **2006**, *81*, 1–22. [CrossRef]
35. Karnieli, A.; Shachak, M.; Tsoar, H.; Zaady, E.; Kaufman, Y.; Danin, A.; Porter, W. The Effect of Microphytes on the Spectral Reflectance of Vegetation in Semiarid Regions. *Remote Sens. Environ.* **1996**, *57*, 88–96. [CrossRef]
36. Saravanan, K.; Saravanan, R. Determination of Water Requirements of Main Crops in the Tank Irrigation Command Area Using CROPWAT 8.0. *Int. J. Interdiscip. Multidiscip. Stud. (IJIMS)* **2014**, *1*, 266–272.
37. Zhu, Y.; Luo, P.; Zhang, S.; Sun, B. Spatiotemporal Analysis of Hydrological Variations and Their Impacts on Vegetation in Semiarid Areas from Multiple Satellite Data. *Remote Sens.* **2020**, *12*, 4177. [CrossRef]
38. Huang, F.; Zhang, D.; Chen, X. Vegetation Response to Groundwater Variation in Arid Environments: Visualization of Research Evolution, Synthesis of Response Types, and Estimation of Groundwater Threshold. *Int. J. Environ. Res. Public Health* **2019**, *16*, 1849. [CrossRef]
39. Halipu, A.; Wang, X.; Iwasaki, E.; Yang, W.; Kondoh, A. Quantifying Water Consumption through the Satellite Estimation of Land Use/Land Cover and Groundwater Storage Changes in a Hyper-Arid Region of Egypt. *Remote Sens.* **2022**, *14*, 2608. [CrossRef]
40. Wei, S.; Xu, T.; Niu, G.Y.; Zeng, R. Estimating Irrigation Water Consumption Using Machine Learning and Remote Sensing Data in Kansas High Plains. *Remote Sens.* **2022**, *14*, 3004. [CrossRef]
41. Basack, S.; Loganathan, M.K.; Goswami, G.; Khabbaz, H. Saltwater Intrusion into Coastal Aquifers and Associated Risk Management: Critical Review and Research Directives. *J. Coast. Res.* **2022**, *38*, 654–672. [CrossRef]
42. Nigatu, Z.M.; Fan, D.; You, W.; Melesse, A.M.; Pu, L.; Yang, X.; Wan, X.; Jiang, Z. Crop Production Response to Soil Moisture and Groundwater Depletion in the Nile Basin Based on Multi-Source Data. *Sci. Total Environ.* **2022**, *825*, 154007. [CrossRef]